

Structural and mass transport properties of liquid ytterbium in the temperature range 1123 K-1473 K

D D Satikunvar, N K Bhatt, and B Y Thakore

Citation: Chin. Phys. B, 2023, 32 (**6**): 067101. DOI: 10.1088/1674-1056/ac8cd9
Journal homepage: http://cpb.iphy.ac.cn; http://iopscience.iop.org/cpb

What follows is a list of articles you may be interested in

Investigation of transport properties of perovskite single crystals by pulsed and DC bias transient current technique

Juan Qin(秦娟), Gang Cao(曹港), Run Xu(徐闰), Jing Lin(林婧), Hua Meng(孟华), Wen-Zhen Wang(王文贞), Zi-Ye Hong(洪子叶), Jian-Cong Cai(蔡健聪), and Dong-Mei Li(李冬梅)
Chin. Phys. B, 2022, 31 (**11**): 117102. DOI: 10.1088/1674-1056/ac7864

Intrinsic V vacancy and large magnetoresistance in $V_{1-\delta}Sb_2$ single crystal

Yong Zhang(张勇), Xinliang Huang(黄新亮), Jinglei Zhang(张警蕾), Wenshuai Gao(高文帅), Xiangde Zhu(朱相德), and Li Pi(皮雳)
Chin. Phys. B, 2022, 31 (**3**): 037102. DOI: 10.1088/1674-1056/ac3070

Electric and thermal transport properties of topological insulator candidate LiMgBi

Hao OuYang(欧阳豪), Qing-Xin Dong(董庆新), Yi-Fei Huang(黄奕飞), Jun-Sen Xiang(项俊森), Li-Bo Zhang(张黎博), Chen-Sheng Li(李晨圣), Pei-Jie Sun(孙培杰), Zhi-An Ren(任治安), and Gen-Fu Chen(陈根富)
Chin. Phys. B, 2021, 30 (**12**): 127101. DOI: 10.1088/1674-1056/ac009f

Anisotropic thermoelectric transport properties in polycrystalline $SnSe_2$

Caiyun Li(李彩云), Wenke He(何文科), Dongyang Wang(王东洋), and Li-Dong Zhao(赵立东)
Chin. Phys. B, 2021, 30 (**6**): 067101. DOI: 10.1088/1674-1056/abeee1

Vanadium based XVO_3 (X=Na, K, Rb) as promising thermoelectric materials: First-principle DFT calculations

N A Noor, Nosheen Mushahid, Aslam Khan, Nessrin A. Kattan, Asif Mahmood, Shahid M. Ramay
Chin. Phys. B, 2020, 29 (**9**): 097101. DOI: 10.1088/1674-1056/ab99ad

---

Structural and mass transport properties of liquid ytterbium in the temperature range 1123 K–1473 K

D D Satikunvar[1,†], N K Bhatt[2], and B Y Thakore[1]

[1] *Department of Physics, Sardar Patel University, Vallabh Vidyanagar, Gujarat* 388120, *India*
[2] *Department of Physics, Maharaja Krishnakumarsinhji Bhavnagar University, Bhavnagar, Gujarat* 364001, *India*

(Received 11 April 2022; revised manuscript received 9 August 2022; accepted manuscript online 26 August 2022)

We have studied the structural and atomic transport properties of liquid f-shell Yb in the temperature range 1123 K–1473 K. Pair interactions between atoms are derived using a local pseudopotential. The potential parameters are fitted to the phonon dispersion curve at room temperature. The local pseudopotential used in the present study is computationally more efficient with only three parameters, and it is found to be transferable to the liquid phase without changing the parameters. Since the various computed properties agree with reported theoretical and experimental findings, the adopted fitting scheme is justified. As a significant outcome of the study, we find that (i) the melting in Yb is governed by the Lindemann's law, (ii) the mass transport mechanism obeys the Arrhenius law, (iii) the role of the three-particle correlation function in deriving the velocity autocorrelation function is small, (iv) the mean-square atomic displacement is more sensitive to the choice of interaction potential than the other bulk properties, and (v) liquid Yb does not show liquid–liquid phase transition within the studied temperature range. Further, due to the good description of the structural and mass transport properties, we propose that Yb remains divalent at reduced density.

Keywords: transport properties, pseudopotential, single-particle dynamics, ytterbium

PACS: 61.25.Mv, 71.20.Eh, 66.10.cg, 71.15.Dx **DOI:** 10.1088/1674-1056/ac8cd9

1. Introduction

The f-shell metal Yb has unique thermophysical and chemical properties such as low elastic modulus, gradual divalent-to-trivalent electronic transition on compression, and low Debye and melting temperatures. Conventionally, it is used as a dopant to improve the strength, grain refinement, and other mechanical properties of stainless steel[1] or in high-power double-clad fiber lasers.[2] The temperature-dependent low elastic properties of Yb are also exploited to form soft Yb-based bulk metallic glass (BMG).[3] The resultant Yb-based BMG shows a low Poisson ratio, a characteristic that is very similar to its liquid phase.[4,5] The itinerant character of 4f electrons under high pressure causes amorphous-to-amorphous phase transition in Yb-based BMGs.[6] These glasses are synthesized by first melting the base elements and then by quenching the melts. It is therefore desirable to know the structural, thermodynamic, and transport properties of liquid Yb, which govern the mechanical and structural properties of the Yb-based BMGs. The physical properties can then be tailored by varying the Yb concentration. Despite such diverse uses of Yb, only limited attempts have been made to explore the liquid phase of Yb, and the general reason can be attributed to the following.

The situation of atomic distribution in liquids is different from that in gaseous and crystalline solid states. The extremes of atomic distributions, e.g., perfect random motion in a gaseous state to bounded near-harmonic motion in a periodic potential well in the solid phase, can be studied with statistical models and available computational codes. In contrast, the distribution of atoms in a liquid is irregular compared to in a crystal and shows short-range order close to the nearest-neighbor region.[7] Another essential aspect of theoretical treatment for the liquid phase is proper choice of the interatomic interaction potential. As evidenced from the short-range order, it is much stronger than the gas phase and quite similar to the solid phase. The delocalized f-shell electron and substantial hybridization effect pose additional challenges for lanthanides in modeling the interaction potential. This ambiguous situation deters one from constructing a standard model to examine the structural aspect of the liquid state of f-shell blocks of the periodic table. Molecular dynamics (MD) simulation is a robust computational scheme to study various properties in a liquid state.[8–15] Although quantum MD (Q-MD) simulations can deduce structural and thermodynamic properties that are fairly consistent with the experimental findings, the number of atoms that can be handled by the Q-MD simulations is still limited. They are also computationally expensive.[16] In contrast, the results derived using classical MD (C-MD) are sensitive to the choice of interaction potential.[17,18]

From a theoretical viewpoint, a simple way to study liquid metals is to consider them as a mixture of ions (ion cores) and valence electrons.[19,20] This forms the concept of the pseudopotential (local or non-local) theory to describe various properties of liquid metals. Although non-local pseudopo-

†Corresponding author. E-mail: dhavalsatikunvar@gmail.com

© 2023 Chinese Physical Society and IOP Publishing Ltd

tentials are preferred over local pseudopotentials, local pseudopotentials are simple to implement. They are found to be highly successful in nearly-free-electron (NFE) systems like alkalis and alkaline metals in examining electrical, thermodynamic, and structural properties.[21–25] Few attempts have been made for transition and rare-earth liquid metals.[26–29] The major complication is treating sp–d–f hybridization of electrons with core–shell electrons and proximity of Fermi energy to valence electrons.[30,31] Furthermore, core–core repulsion is also vital while deriving the lattice dynamical properties. However, according to the generalized pseudopotential theory, it is possible to treat the transition and f-shell metals on an equal footing by assuming effective valence as an adjustable parameter.[32–37] An important feature in treating the liquid metals within such empirical local pseudopotential formalism is the determination of the potential parameters. In our recent paper,[38] we have deduced the effect of phonon anharmonicity and electron free energy on the thermodynamic properties of fcc Yb within the density functional theory (DFT). It appears for Yb that Lindemann's criterion is applicable within the prescribed accuracy, and as elaborated below, it is sensible to deduce the potential parameters from the vibrational response of the materials. In the present study, the pseudopotential parameters are determined by fitting the experimental[39] and DFT-based phonon dispersion relation[38] at room temperature (RT). Once the pseudopotential parameters were obtained, they were kept constant for further calculations. We studied structural, atomic mass transport and dynamical properties such as mean-square displacement (MSD) and the velocity autocorrelation function (VACF) at different liquid temperatures. These results are compared and discussed with the available experimental and embedded atom potential (EAM)-based findings.[40]

The paper is organized as follows. The following section briefly outlines the basic theory and describes the parametrization scheme. In Section 3, the results for various physical properties are discussed and compared with the available findings. The last section describes the major inferences drawn from the study. We follow the atomic unit system: $\hbar = 1$, $e^2 = 2$, energy in Ry, and distance measured in Bohr radius, $a_0 = 1$ unit.

2. Theoretical formalism

2.1. Interaction potential

The pseudopotential method within the linear response theory for interacting electron gas is one of the simplest but most effective methods to describe static, dynamic, thermodynamic, and transport properties of metals.[19,20] A proper account of potential parameters provides almost as accurate a finding for various physical properties in a wide range of solid and liquid temperatures as using first-principles DFT-based results.[21–29,41,42] At the melting point, solid and liquid phases coexist in equilibrium. This first-order phase transition is described by the widely used phenomenological Lindemann criterion.[43] A refined version of this[44–46] gives the physical elucidation of the law and relates the melting temperature to entropy[47] and anharmonic lattice vibrations.[45] According to Lawson,[46] it is possible to determine the melting temperature from the knowledge of elastic energy. In this presentation, the amplitude of thermal lattice vibration can be given by

$$\langle u^2 \rangle = \frac{3\hbar^2 T}{M k_{\mathrm{B}} \theta_{\mathrm{e}}^2}. \tag{1}$$

Here,

$$\theta_{\mathrm{e}} \equiv \frac{\hbar}{k_{\mathrm{B}}} \left\{ \frac{1}{M} \frac{\partial^2 E_{\mathrm{e}}(R)}{\partial R^2} \right\}^{1/2}$$

represents the characteristic temperature corresponding to the elastic part of the energy E_{e}, T is absolute temperature, M is the mass of a metal atom and k_{B} is the Boltzmann constant. According to the Lindemann law, melting occurs when the root-mean-square vibration amplitude exceeds a threshold value (ranging between 0.05 and 0.2) of the fraction of interatomic distance a_0, i.e., $\sqrt{\langle u^2 \rangle} = C_{\mathrm{L}} a_0$, C_{L} being the Lindemann constant. In our previous paper, we reported the thermophysical properties of Yb in the fcc phase[38] up to normal melting temperature ($T_{\mathrm{M}} = 1100$ K) by combining self-consistent DFT calculations with the anharmonic phonon contribution. Having obtained the total Helmholtz free energy $F(V, T_{\mathrm{M}})$, including the phonon anharmonic part,[38] we can estimate C_{L} as follows. Following Joshi *et al.*,[48,49] we have computed the effective vibrational force constant at T_{M} and thereby determined θ_{e} on replacing E_{e} by $F(V, T_{\mathrm{M}})$. Finally, an equilibrium lattice constant a_0 corresponding to T_{M} is used to find the Lindemann constant. It is found to be 6.02% of a_0 at melting, which is within the prescribed accuracy of Lindemann's criterion. This proposes that Yb can be treated with other simple metals where Lindemann's criterion is valid. This also advocates that the lattice dynamical part of the free energy governs the melting scenario in Yb and recommends that the potential parameters fitted through the phonon dispersion curve (PDC) can be beneficial to describing the liquid phase near the melting temperature.

The phonon frequencies are the eigenvalues of a dynamical matrix with matrix elements composed of ion–ion interaction, the repulsive term due to the core and electron–ion interactions. It is given by

$$D_{\alpha\beta}(q) = \sum_n \left(1 - \mathrm{e}^{-\mathrm{i}qr}\right) \left(\frac{\partial^2 V_{\mathrm{eff}}(r)}{\partial r_\alpha \partial r_\beta} \right)_{r=r_n}. \tag{2}$$

Here, subscripts α and β denote the Cartesian components, $V_{\mathrm{eff}}(r)$ is the effective interatomic potential at separation r,

and q represents the magnitude of the wave-vector. We compute the electron–ion interaction using the model potential proposed by Baria *et al.*[50] The following equation gives the bare-ion interaction in r-space:

$$w(r) = \begin{cases} -\dfrac{ze^2 r}{r_c^2}\left(2 - e^{\left(1-\frac{r}{r_c}\right)}\right), & r < r_c, \\ -\dfrac{ze^2}{r}, & r \geq r_c. \end{cases} \quad (3)$$

Unlike an empty-core pseudopotential, which is frequently used for NFE systems, in the above equation, the authors[50] have assumed a non-zero analytic term inside the core ($r < r_c$), which is zero and has a finite slope as $r \to 0$. However, they retain the Coulombian repulsion outside the core. The physical justification of the potential can be given as follows. The rare earth metals have unfilled d- and f-bands, in which lanthanides possess incomplete 4f-bands. However, it is believed that 4f-electrons in lanthanides are mostly localized (less itinerant), and they can be treated as on par with other regular d-band transition metals. Furthermore, metals such as Th[51] and presumably Yb also have broad d-bands similar to the s- and p-bands in simple metals. This allows the use of simple metal pseudopotential modified to encompass the specific features of transition metals. Modification within the core region, due to non-perfect orthogonalization cancellation between conduction bands and valence bands, has thus improved the d-band description and given accurate results for lattice dynamics and several other bulk properties for f-shell metals.[50] The net pair interaction is expressed as the sum of direct Coulomb repulsive interaction between ions and an attractive indirect interaction mediated through valence electrons. The indirect interaction, also known as the band structure energy, includes the exchange and correlation effect. Thus, in a sense, the indirect interaction plays the same role as the embedding term in EAM-based potential[40] and provides necessary binding to the system. In the EAM potentials, however, the pair-wise term is frequently treated by empirical cubic- or higher-order polynomials in interatomic separation, whose coefficients are determined by fitting several observed physical properties. Finally, a Born–Mayer-type term is used to account for s–d–f hybridization and repulsion between the ion cores.[52] The resultant pair interaction is then described as follows:

$$V_{\text{eff}}(r) = \frac{z^2 e^2}{r} + \frac{\Omega_0}{\pi^2}\int F(q)\left[\frac{\sin(qr)}{qr}\right] q^2\,\mathrm{d}q + \alpha' e^{-\gamma r}. \quad (4)$$

Here, $F(q)$ represents the energy wave-number characteristics, which couples the bare ion interaction and the Hartree exchange and local-field correction term for valence electrons. In the present study, the local-field correction for interacting electron gas is described within the linear response theory given by Ichimaru and Utsumi.[53] It satisfies the necessary self-consistency condition in the compressibility sum rule along with the short-range corrections. Complete details of the mathematical formalism can be found elsewhere, e.g., Ref. [54]. The dynamical matrix can now be solved to determine the phonon frequency using the effective pair interaction, Eq. (4). The only pseudopotential parameter r_c and the Born–Mayer parameters (α' and γ) are tuned to optimize the PDC at RT equilibrium volume with experimental[38] and DFT-based results.[39] These parameters are given in Table 1, and they are used for the entire range of temperature that we explore in the study.

Table 1. Input parameters.

z	r_c (a.u.)	α' (Ry)	γ
2	2.2184	268.81	1.90

2.2. Structural properties

Virtually all liquid state properties require structural information about the wandering atoms. Thus, the static structure factor $S(q)$, the Fourier transform of pair-distribution function $g(r)$, is essential in the liquid state theory. For the case of liquid metals, a relatively soft-sphere reference system, e.g., the charged hard sphere (CHS), is preferred. We employ CHS to find $S(q)$ and $g(r)$. Complete computational details can be referred to in Refs. [55–57]. Following Palmer and Weeks,[58] we calculate $S(q)$ using the CHS as a reference system employing the mean-spherical approximation.

2.3. Dynamical and transport properties

Since an exact solution of the time–space correlation functions by solving the Liouville equation is practically impossible, one must employ some unavoidable approximations. One of the simplest ways to approach the dynamics of liquid metals is to examine the VACF, $\psi(t)$. The computation $\psi(t)$ requires a proper account of the screening, caging, and collective effects of the constituent particles.[7] To this end, Frenkel[59] used the concept of relaxation time τ which is the average time between two consecutive equilibrium arrangements in a given thermal condition. Thus, a liquid can be visualized as a many-body system fragmented into vibrational and stable packing parts. Depending upon the strength of the interaction potential and local minima in an energy hypersurface, atoms jump from one potential well to the nearest next one. This hopping frequency is given by the inverse of relaxation time, τ^{-1}. After each successive jump, an atom acquires an equilibrium position in a respective potential well. It is then reasonable to assume that in every potential well, an atom performs near-harmonic motion with the characteristic frequency ω. An important valid assumption in this approach is that during a very short time period τ the liquid structure remains unchanged, and the binary collisions can describe the waiting time for the jump to the next potential well between the atoms. According to Tankeshwar *et al.*,[60] the binary term

can be described by a hyperbolic secant function, whereas the near-harmonic oscillations in a given potential well are given by $\cos(\omega t)$. Thus,

$$\psi(t) = \operatorname{sech}\left(\frac{t}{\tau}\right)\cos(\omega t). \tag{5}$$

Again, we refer readers to Ref. [60] for the complete computational details. The self-diffusion coefficient (D) is then derived using the Green–Kubo approximation

$$D = \frac{k_B T}{M}\int_0^\infty \psi(t)\,\mathrm{d}t. \tag{6}$$

The viscosity and MSD at different temperatures are also calculated from the knowledge of VACF.[7]

3. Results and discussion

The input potential parameters for optimizing the PDC at RT equilibrium lattice constant are given in Table 1. The difference in parameters between Baria *et al.*[50] and the present study is attributed to the different exchange and correlation function forms and the fitting procedure. The computed results for PDC, along with the DFT-based theoretical results[38] and experimental findings,[39] are shown in Fig. 1. A good agreement for longitudinal and transverse branches is found along the high-symmetry directions in the first Brillouin zone (BZ). This is quite suggestive and justifies the use of local pseudopotential in treating the vibrational response of f-shell Yb. As discussed in the preceding section, Yb, like Th,[30] behaves as a simple metal where the d- and f-bands do not sensitively affect the bulk properties. However, this proposition should be carefully checked for electronic transport properties. PDC deduced using the EAM potential[40] is also shown for comparison. The author[40] has deduced the EAM parameters by fitting elastic, cohesive, and phonon dynamical properties. These results also agree with reported findings.

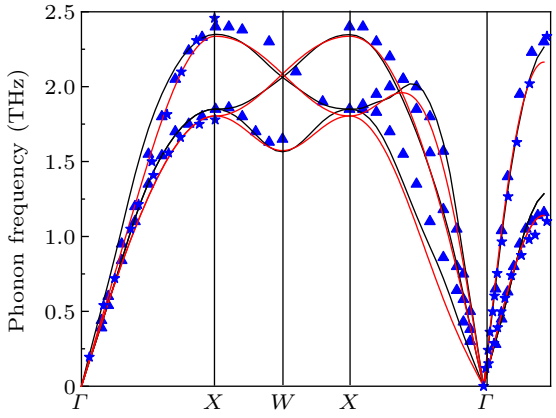


Fig. 1. Phonon dispersion curve (black line) of Yb at RT along with DFT result (red line),[38] experimental circles[39] and stars due to EAM potential.[40]

In the liquid state, interaction between the atoms is slightly weaker than in the solid phase; nonetheless, the motion of atoms strongly depends on the interaction between them. The presently calculated results for pair potential are shown in Fig. 2 at different densities (= temperatures), where the inset enlarges the effect of density. We used reported data for density[61] and thereby derived atomic volumes corresponding to each temperature ranging from 1123 K to 1473 K. Since the stability of an atom depends on the depth of the potential well, it is clear from Fig. 2 that as the temperature increases, the depth of the potential well decreases. This is clear evidence of a decrease in binding with temperature. Further, we notice that the minimum potential point remains almost fixed, but the potential well becomes broader.

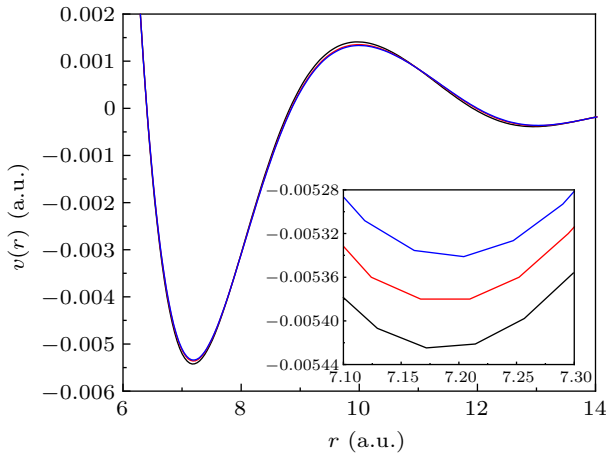


Fig. 2. Pair potential of liquid Yb at different temperatures. Black (T = 1123 K), red (T = 1273 K), and blue (T = 1473 K).

In the present study, the structure factor has been calculated using the CHS method,[58] and numerical results are compared in Fig. 3. The CHS scheme depends on the packing fraction η and the Coulomb parameter Γ. Theoretically, they are related to pair potential and effective valence (z) and vary with atomic volume and temperature.[55–57] The temperature-dependent hard-sphere diameter σ and hence the packing fraction η are estimated using the $V_{\mathrm{eff}}(\sigma) = \frac{1}{2}k_B T + V_{\mathrm{eff}}^{\min}(r)$ criterion. Here, $V_{\mathrm{eff}}^{\min}(r)$ represents the minimum (principal dip) in the effective pair interaction potential. The Coulomb parameter is computed by the relation $\Gamma = (Ze)^2/(\sigma k_B T)$ at each temperature with corresponding atomic volume. We assume that Yb remains divalent in the entire temperature range. The experimental result for the structure factor obtained by Waseda[61] matches very well with our data. It is interesting to note that the temperature dependency of the packing fraction given by Waseda,[61] which is based on the hard-sphere model, is almost identical in the present case. Both show a decreasing trend with temperature. This suggests that the structure in liquid Yb near the melting temperature is primarily governed by the hard-sphere diameter. Nevertheless, the CHS model also depends on the Coulomb coupling parameter Γ. We observe a broadening of a principal peak for $S(q)$ and a decrease in its height as temperature increases. It is clear from the study that the peak position for $S(q)$ remains almost fixed. Similarly, the

second-peak position also remains the same. Compared to the first peak, the second peak for all temperatures is broad and smaller. Other theoretical results for $S(q)$ due to EAM potential overestimate the present data. Recently, Khusnutdinoff *et al.*[62] have also noted such a discrepancy for liquid Li and found that the results using the pseudopotentials are in better agreement than the EAM-based pair interaction.

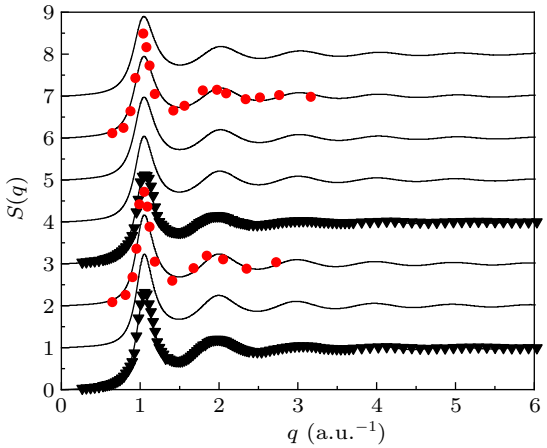


Fig. 3. Structure factor of liquid Yb at different temperatures. From bottom (1123 K) to top (1473 K) in steps of 50 K. Each graph is raised by unity. Experimental findings (triangles) due to Waseda[61] and EAM-based results (circles) at 1200 K and 1400 K are from Ref. [40].

The pair correlation function $g(r)$ is shown in Fig. 4 along with experimental[61] and other theoretical findings.[26] Since $g(r)$ represents the probability of finding atoms, given the central atom, the largest probability is at a distance where the attractive force is maximum. The maximum discrepancy in peak position and related magnitude in the present $g(r)$ with respect to the experiment in Ref. [61] are 3.5% and 4.5%, respectively. These results are presented in Table 2 and other reported findings.[26,61] We have also noted that the ratio of peak position and related magnitude for $S(q)$ changes, but the same for $g(r)$ remains constant with temperature. This observation follows the results for pair potentials in Fig. 2. Since the first-peak position correlates with the principal dip in the interaction potential, an almost fixed dip-position in pair potential is indicative. According to the free-volume theory,[23,24] in a liquid without any phase transition, a decrease in density is due to the lowering of the coordination number and not the increase in interatomic separation. This fact is confirmed from the numerical results for the coordination number (n_1) as a function of temperature (see Table 3). It decreases linearly with temperature. Thus, the free volume available to the wanderer atom increases at higher temperatures due to the reduction in near-neighbor atoms. Again, the present results are in better agreement with experimental[61] data than the EAM-based findings.[40] There is a systematic right shift for the first peak in $g(r)$ in Ref. [40]. Since the ratio of first-peak position to second varies by 1.4% (1.868–1.884), we confirm that Yb behaves like a normal liquid in the studied temperature range.

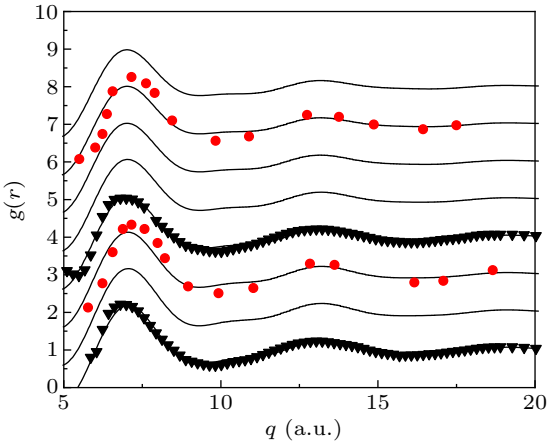


Fig. 4. Same as Fig. 3 but for pair correlation function.

Table 2. Peak position and related magnitude of $g(r)$ for liquid Yb.

T (K)	First peak in $g(r)$				Second peak in $g(r)$				r_2/r_1	$g(r_2)/g(r_1)$
	r_1 (a.u.)		Magnitude		r_2 (a.u.)		Magnitude			
1123	7.0318	6.803[61], 6.960[26]	2.1166	2.214[61], 2.518[26]	13.1373	13.039[61], 13.480[26]	1.2238	1.234[61], 1.238[26]	1.8683	0.5782
1173	7.0298		2.0895		13.1486		1.2148		1.8704	0.5814
1223	7.0246		2.0657		13.1605		1.2067		1.8735	0.5842
1273	7.0445	6.803[61], 6.93[26]	2.0424	2.034[61], 2.359[26]	13.1979	13.228[61], 13.53[26]	1.1992	1.215[61], 1.202[26]	1.8735	0.5872
1323	7.0221		2.0049		13.1932		1.1876		1.8788	0.5923
1373	7.0391		1.9789		13.2248		1.1790		1.8788	0.5958
1423	7.0133		1.9599		13.2141		1.1731		1.8841	0.5986
1473	7.0327		1.9356		13.2507		1.1657		1.8842	0.6022

Table 3. Coordination number (n_1) for liquid Yb.

T (K)	1123	1173	1223	1273	1323	1373	1423	1473
n_1	10.01, 10.3[61]	9.35	8.51	7.95	7.16	6.52	6.01	5.62

The computed results of normalized VACF for liquid Yb at different temperatures are shown in Fig. 5. The term contributing the fourth-order sum rule in the expression for VACF depends on the static three-particle correlation function.[60] However, in a similar calculation for liquid Sn,[24] and as noticed in Ref. [63], the contribution due to this term is minimal and decreases further with temperature. This allows us to treat this term as a small (constant) parameter whose value is de-

termined once and for all at melting temperature. Initially, the VACF falls rapidly and attains a negative value. The binary collision term, sech (t/τ), determines this region. The negative region progressively decreases with temperature. Such behavior can be understood as follows. At short distances, an atom in the liquid experiences a repulsive force due to the surrounding atoms, and backscattering occurs. With a rise in temperature, the interaction between atoms weakens, and the free volume available to wandering atoms increases. This, together, reduces the negative region in the VACF. The strength of the near-harmonic pair interaction (potential well in the energy hypersurface) compared to the gaseous phase at near-neighbor distance results in oscillation in the VACF at finite time, which also decreases with temperature. However, compared to the EAM-based results,[40] though oscillating in-phase with our findings, these results show stronger damping.

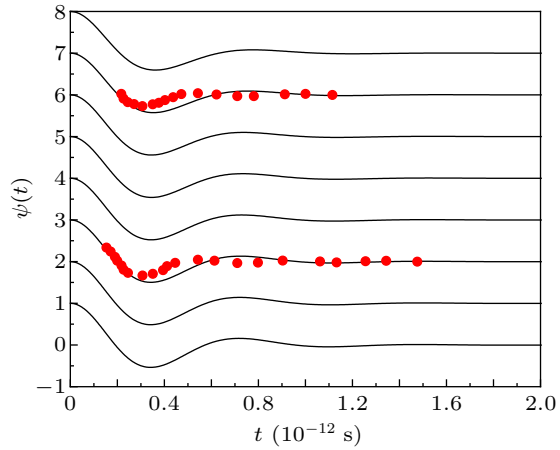


Fig. 5. VACF of liquid Yb at different temperatures. From bottom (1123 K) to top (1473 K) in steps of 50 K. Except for the 1123 K graph, each graph is raised by unity. Theoretical findings (circles) from Ref. [40] are for $T = 1200$ K and 1400 K.

The self-diffusion coefficient is computed using the knowledge of VACF, and numerical results are displayed in Fig. 6 along with experimental[64] and theoretical findings.[40,65] Overall good agreement is found for the entire temperature range reported in the present study. The maximum deviation in the present calculation for diffusion coefficient lies within 2% with the experimental findings. Moreover, we observe that Yb atoms follow the Arrhenius law. Thus, the activation energy can be calculated through the logarithmic dependency of the diffusion coefficient on the temperature. We find the activation energy to be 21.84 kcal/mol, which is in fair agreement with the 28.9 kcal/mol value predicted by Dariel[66] in the bcc phase, just before melting. We have also reported in Fig. 7 the calculated shear viscosity as a function of temperature using the Stokes–Einstein (SE) relation. Though viscosity can be directly deduced from the simulation, we have used the SE relation. The SE relation holds as long as the term $(D\eta/T)$ remains constant. We have found that liquid Yb in the studied temperature range gives a constant $(D\eta/T)$ ratio. The corresponding effective radius lies between 1.10 Å and 1.13 Å. In a recent study on noble metals,[67] the authors confirmed the validity of the SE equation. We do not find any direct comparison for viscosity (due to the inaccessibility of Ref. [64]) at higher temperatures. Nevertheless, the present estimate follows a theoretical datum[68,69] close to the melting temperature, including the EAM-based finding.

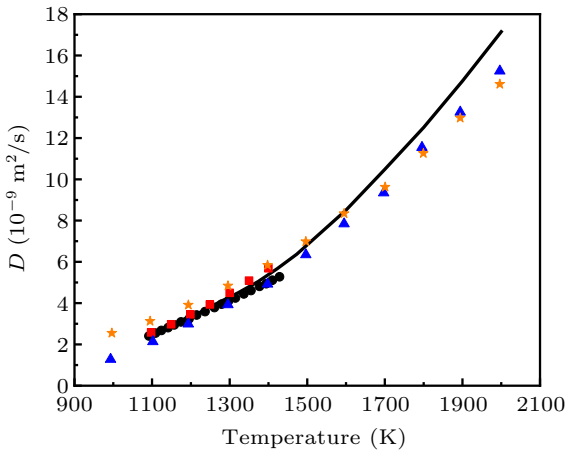


Fig. 6. Self-diffusion coefficient of liquid Yb as a function of temperature. Experimental findings (squares),[64] theoretical findings (triangles) due to Ref. [40], Green–Kubo formalism (stars)[40] and circle.[65]

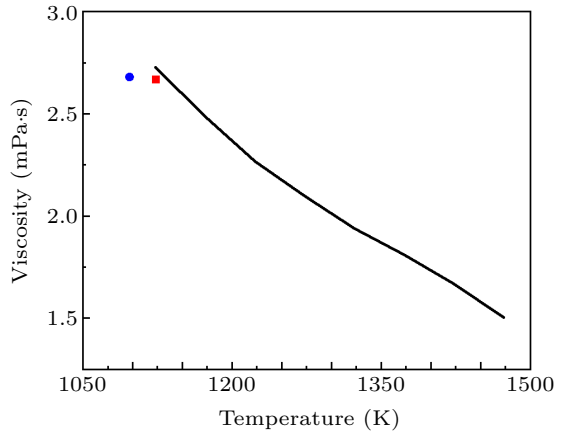


Fig. 7. Viscosity as a function of temperature. Theoretical findings circle[68] and square.[69]

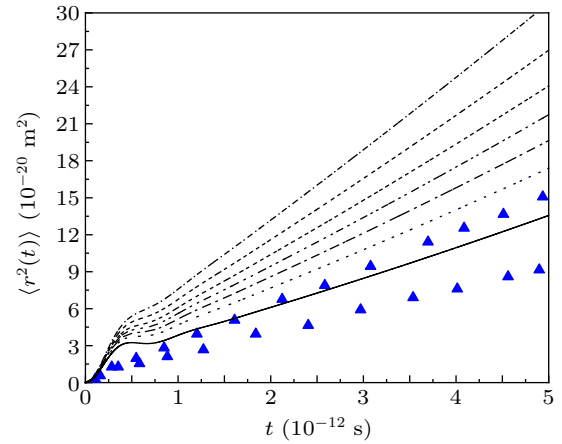


Fig. 8. MSD at different temperatures: bottom (1123 K) to top (1473 K) in steps of 50 K. Theoretical findings (triangles)[40] at 1200 K and 1400 K are also shown.

Finally, we show in Fig. 8, along with the theoretical findings due to EAM-based potential,[40] the results for MSD for the temperature range 1123 K–1473 K. The EAM-based data sets at 1200 K and 1400 K, respectively, strongly differ with present results at 1323 K and 1473 K. The present results do not just overestimate the values but also show large oscillations at small (<1 ps) time (t). This can be attributed to the strength of the pseudopotential-based pair interaction compared to the EAM-based effective pair potential. However, the asymptotic large-t slope (which also estimates the self-diffusion coefficient) is almost identical for both interactions.

4. Summary and conclusion

In summary, we have derived structural and atomic mass transport properties for liquid Yb in the temperature range 1123 K–1423 K using the local pseudopotential,[50] where potential parameters are fitted through phonon dynamics. The fitting scheme appears to be accurate as all studied properties agree with reported theoretical and experimental findings. This corroborates that the melting in Yb is mechanical in origin and governed by Lindemann's law. We infer from self-diffusion and viscosity data that the mass transport mechanism follows the Arrhenius law. A good correlation between EAM-based VACF and the present estimate confirms that the role of the three-particle correlation function is less significant. The MSD is the most sensitive physical property to the choice of interaction potential in the hydrodynamic domain. Temperature variation of coordination number suggests that the liquid Yb does not show liquid–liquid phase transition within the studied temperature range, and Yb is a normal liquid. In comparison, other computed transport and structural properties appear less dependent on the choice of the pair potential as long as the gross behavior of the interaction potential is similar. Although the philosophy in constructing the EAM potential and local pseudopotential is different, numerical results for various properties confirm their validity for the liquid phase. A good overall description of the computed properties, e.g., $S(q)$ and the self-diffusion coefficient, justify the proposition that Yb remains divalent at expanded volume (= reduceddensity). Since the EAM potential[40] depends on several fitting parameters, we propose that the local pseudopotential used in the present study is computationally more efficient. It is found to be transferable to the liquid phase without changing the parameters.

Acknowledgment

DDS and BYT are thankful to the Department of Physics, Sardar Patel University, Vallabh Vidyanagar, Gujarat, India for providing the necessary computing facilities.

References

[1] Hammond C R 2000 *The element, in Handbook of Chemistry and Physics* (CRC Press)
[2] Geong Y, Sahu J K, Pagne D N and Nilsson J 2004 *Opt. Exp.* **12** 6008
[3] Wang J Q, Wang W H and Bai H Y 2009 *J. Appl. Phys. Lett.* **94** 041910
[4] Novikov V N and Sokolov A P 2006 *Phys. Rev. B* **74** 064203
[5] Wang W H 2006 *J. Appl. Phys.* **99** 096506
[6] Wang Y Y, Zhao W, Li G, Li Y C and Liu R P 2013 *Mater. Lett.* **110** 184
[7] Shimoji M 1977 *Liquid Metals: An Introduction to the Physics and Chemistry of Metals in the Liquid State* (Academic Press)
[8] Brooks B R, *et al.* 2009 *J. Comput. Chem.* **30** 1545
[9] Phillips J C, *et al.* 2005 *J. Comput. Chem.* **26** 1781
[10] Case D A, *et al.* 2006 *J. Comput. Chem.* **26** 1668
[11] Spoel D V, Lindahl E, Hess B, Groenhof G, Mark A E and Berendsen H J C 2005 *J. Comput. Chem.* **26** 1701
[12] Christen M, *et al.* 2005 *J. Comput. Chem.* **26** 1719
[13] Smith W, Yong C W and Rodger P M 2002 *Mol. Simu.* **28** 385
[14] Humphrey W, Danke A and Schulten K 1996 *J. Mol. Graph.* **14** 33
[15] Bergman D L, Laaksonen L and Laaksonen A 1997 *J. Mol. Graph.* **15** 301
[16] Zhang J, Fuller J and An Q 2021 *J. Phys. Chem. B* **125** 8876
[17] Patel A B and Sheng H 2020 *Phys Rev. B* **102** 064101
[18] Lynes O, Austin J and Kerridge A 2019 *Phys. Chem. Chem. Phys.* **21** 13809
[19] Harrison W A 1966 *Pseudopotential in Theory of Metals* (New York: Benjamin)
[20] Harrison W A and Wills J M 1982 *Phys. Rev. B* **25** 5007
[21] Bhatt N K 2007 *Thermodynamic properties of some metals at high temperatures* (PhD Thesis, Sardar Patel University)
[22] Patel A B, Bhatt N K, Thakore B Y, Vyas P R and Jani A R 2014 *Phys. Chem. Liq.* **52** 471
[23] Patel A B, Bhatt N K, Thakore B Y, Vyas P R and Jani A R 2014 *Mol. Phys.* **112** 2000
[24] Patel A B, Bhatt N K, Thakore B Y Vyas P R and Jani A R 2014 *Eur. Phys. J. B* **87** 39
[25] Joshi R H, Satikunvar D D, Bhatt N K, Thakore B Y and Jani A R 2016 *Adv. Material. Res.* **1141** 24
[26] Thakor P B, Gajjar P N and Jani A R 2006 *Commun. Theor. Phys.* **46** 337
[27] Thakor P B, Gajjar P N and Jani A R 2002 *J. Phys. Condens. Matt.* **5** 493
[28] Bhatia K G, Bhatt N K, Vyas P R and Gohel V B 2015 *AIP Conf. Proc.* **1665** 110014
[29] Baria J K 2003 *Chin. Phys. Lett.* **20** 894
[30] Rosengren A, Ebbsjo I and Johansson B 1975 *Phys. Rev. B* **12** 1337
[31] Moriarty J A, Benedict L X, Glosli J N, Hood R Q, Orlikowski D A, Patel M V, Söderlind P, Streitz F H, Tang M and Yang L H 2006 *J. Mater. Res.* **21** 563
[32] Moriarty J A, Belak J F, Rudd R E, Söderlind P, Streitz F H and Yang L H 2002 *J. Phys. Condens. Matt.* **14** 2825
[33] Moriarty J A and Widom M 1997 *Phys. Rev. B* **56** 7905
[34] Moriarty J A 1970 *Phys. Rev. B* **1** 1363
[35] Moriarty J A 1972 *Phys. Rev. B* **5** 2066
[36] Moriarty J A 1972 *Phys. Rev. B* **6** 1239
[37] Moriarty J A 1990 *Phys. Rev. B* **42** 1609
[38] Satikunvar D D, Bhatt N K and Thakore B Y 2021 *J. Appl. Phys.* **129** 035107
[39] Stassis C, Loong C K, Theisen C and Nicklow R M 1982 *Phys. Rev. B* **26** 4106
[40] http://sites.google.com/site/eampotentials/Yb
[41] Bhatt N K, Thakore B Y, Vyas P R and Jani A R 2010 *Int. J. Thermophys.* **31** 2159
[42] Bhatt N K, Thakore B Y, Vyas P R and Jani A R 2010 *Phys. B* **405** 3492
[43] Lindemann F A 1910 *Z. Phys.* **11** 609
[44] Gilvary J J 1956 *Phys. Rev.* **102** 308
[45] Lawson A C 2009 *Philo. Manga.* **89** 1757
[46] Vopson M M, Rogers N and Hepburn I 2020 *Solid State Commun.* **318** 113977
[47] Wallace D C 1991 *Proceedings: Mathematical and Physical Sciences* **433** 615

[48] Joshi R H, Bhatt N K, Thakore B Y, Vyas P R and Jani A R 2018 *Comput. Condens. Matter* **15** 79
[49] Joshi R H, Thakore B Y, Vyas P R, Jani A R and Bhatt N K 2017 *Chin. Phys. B* **26** 116502
[50] Baria J K and Jani A R 2010 *Physica B* **405** 2065
[51] Baria J K, Gajjar P N and Jani A R 2002 *Ind. J. Pure Appl. Phys.* **40** 714
[52] Onwuagba B N 1987 *Phys. Status. Solidi. B* **141** 105
[53] Ichimaru S and Utsumi K 1981 *Phys. Rev. B* **24** 7385
[54] Vora A M 2012 *Bulg. J. Phys.* **39** 215
[55] Lai S K, Akinlade O and Tosi M P 1990 *Phys. Rev. A* **41** 5482
[56] Akinlade O, Lai S K and Tosi M P 1990 *Phys. B* **167** 61
[57] Lai S K 1985 *Phys. Rev. A* **31** 3886
[58] Palmer R G and Weeks J D 1973 *J. Chem. Phys.* **58** 4171
[59] Frenkel D Luijin F and Binder P M 1992 *Eur. Phys. Lett.* **20** 7
[60] Tankeshwar K, Singla B and Pathak K N 1991 *J. Phys. Condens. Matt.* **3** 3173
[61] Waseda Y 1980 *The Structure of Non-Crystalline Materials* (MacGraw: New York)
[62] Khusnutdinoff R M, Galimzyanov B N and Mokshin A V 2018 *J. Expert. Theor. Phys.* **126** 83
[63] Wallace D C 1997 *Phys. Rev. E* **56** 1981
[64] Wittenberg L J and DeWitt R 1973 *Viscosity of Liquid Rare-Earth and Actinide Metals* (In *Proc. of the Second Int. Conf. on the Properties of Liquid Metals* (London: Taylor))
[65] Postovalov V G, Romanov E P and Kondrat'ev V P 2009 *Phys. Met. Meta.* **107** 1
[66] Dariel M P *Handbook on the Physics and Chemistry of Rare Earths* (North-Holland Publishing Company: Netherlands)
[67] Khatun M N and Gosh R C 2021 *Phys. Lett. A* **403** 127385
[68] Battezzati L and Greer A L 1989 *Acta Metall.* **37** 1791
[69] Hirai M 1993 *Isij Inter.* **33** 251